Supporting Information

Self-rectifying Bipolar Resistive Switching Memory Based on an Iron Oxide and Graphene Oxide Hybrid

Se-I Oh,[a] Janardhanan R. Rani,[b] Sung-Min Hong,[b] and Jae-Hyung Jang*[a, b, c]

[a]*Department of WCU Nanobio Materials and Electronics, Gwangju Institute of Science and Technology, 123 Cheomdangwagi-ro, Buk-gu, Gwangju, 500-712, South Korea.*

[b]*School of Electrical Engineering and Computer Science, Gwangju Institute of Science and Technology, 123 Cheomdangwagi-ro, Buk-ju, Gwangju, 500-712, South Korea.*

[c]*Research Institute for Solar and Sustainable Energies, Gwangju Institute of Science and Technology, 123 Cheomdangwagi-ro, Buk-gu, Gwangju, 500-712, South Korea.*

**E-mail: jjang@gist.ac.kr, Tel: +82-62-715-2209*

Contents

1. FeO_x-GO film characterization

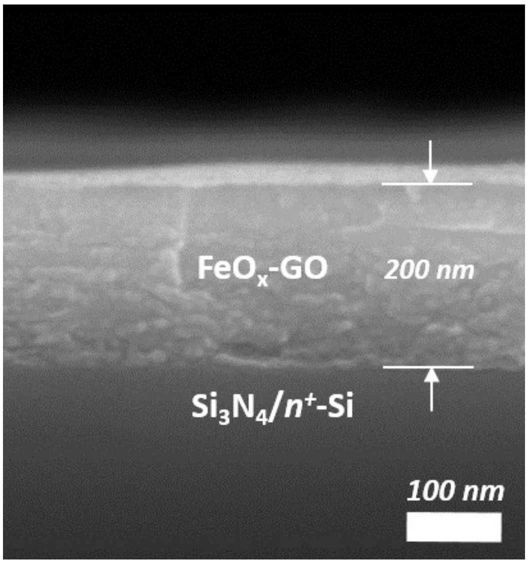

Fig. S1 Cross-sectional scanning electron microscope image of the memory device before deposition of Au/Ni metal electrode: The thickness and the root mean square surface roughness of FeO_x-GO film are 200 nm and 3.41 nm, respectively.

Table S1 The Hall measurement results of the FeO_x-GO film annealed at 90°C for 60 minutes. N-type conduction in the FeO_x-GO film is confirmed by the minus sign of the sheet Hall coefficient.

	Electron mobility (cm^2/Vs)	**Electron concentration (cm^{-3})**	**Sheet resistance (Ω/sq)**
FeO_x-GO film	153	9.33×10^{13}	8.73×10^{6}

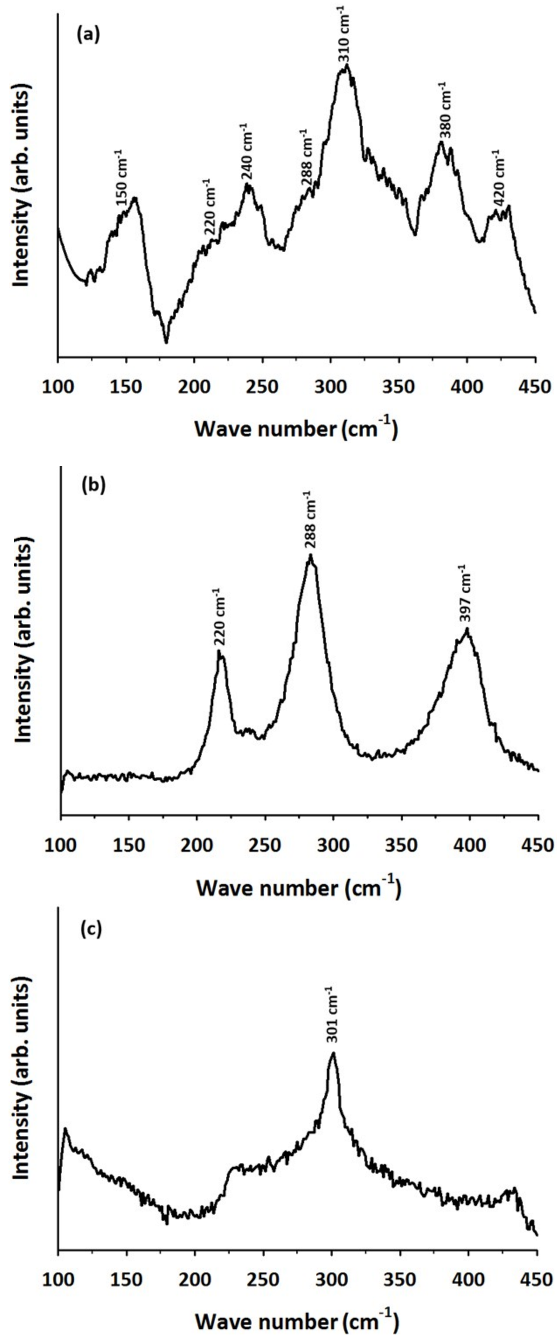

Fig. S2 Raman spectra of (a)Ni/FeO_x-GO/Si_3N_4/n^+-Si, (b)FeO_x-GO/Si_3N_4/n^+-Si, and (c)Ni/GO/Si_3N_4/n^+-Si samples.

Raman bands observed at 240 cm^{-1} and 310 cm^{-1} in Fig. S2a confirm the presence of Ni-O-Fe bonds in the FGSN/n^+ device.[1] Raman bands at 220 cm^{-1} and 288 cm^{-1} in Fig. S2a-b correspond to Fe-O bonds.[2] The Raman band at 301 cm^{-1} in Fig. S2c is due to the characteristics of crystalline Si substrate.[3]

2. Temperature dependent *I-V* characteristics of FGSN/n^+ device

The current-voltage-temperature (*I-V-T*) characteristics of the FGSN/n^+ device were measured in the temperature range 303–363 K. The *I-V-T* characteristics at voltages ranging from 5.3 to 6.5 V for the HRS were fitted with the P-F emission equation in the inset of Fig. S3. The linear relation in ln (*J/E*)-(1/*kT*) suggests that P-F emission is the dominant current conduction mechanism in this voltage region.[4] The trap depth ($q\phi_{PF}$) extracted from the slope of the fitted lines ranged between 0.93 and 0.99 eV, which matches well with the reported values.[5,6]

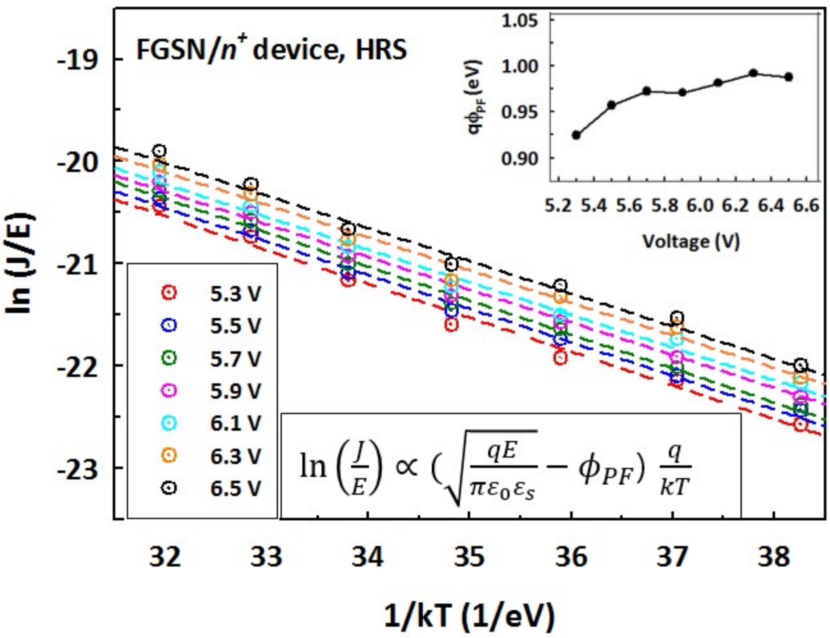

Fig. S3 The ln (*J/E*)-(*1/kT)* plot at the voltages ranging from 5.3 to 6.5 V. In the inset equation, *J, E,* ϕ_{PF}, ε_0, and ε_s stand for the current density, the electric field applied on the active layer, the barrier height of trap, vacuum permittivity, and relative permittivity, respectively. The inset figure is the trap depth ($q\phi_{PF}$) in P-F emission at each voltage in the HRS.

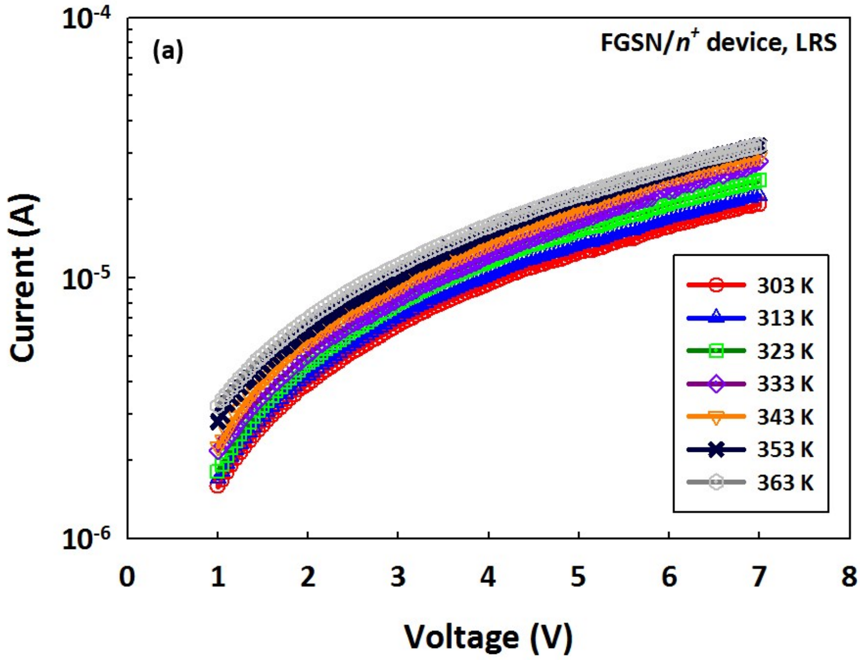

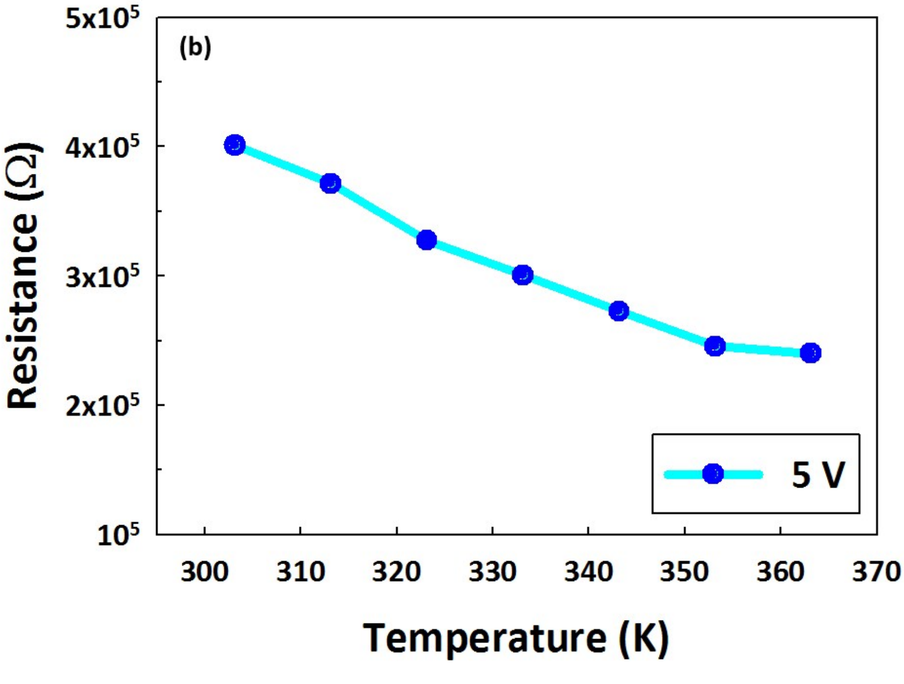

Fig. S4 a) Temperature dependent *I-V* characteristics of the FGSN/n^+ device in the LRS at the voltages ranging from 1.0 to 7.0 V, and b) The temperature dependent LRS resistance of FGSN/n^+ device at the applied bias voltage of 5 V, which is consistent with that of TAT conduction model.[7]

3. Conduction mechanism of FGSN/n^+ device in negative bias region

The conduction mechanism of the FGSN/n^+ device under the negative bias was analyzed. The *I-V-T* characteristics at the voltages ranging from −1.4 to −2.1 V (Fig. S5a) exhibit current increases with temperature. The log |*I*|-log |*V*| graph at voltage ranging from −0.1 to −2.1 V (inset of Fig. S5a) has a slope of 1. These results suggest that the current conduction in this voltage region is governed by the trap-assisted hopping mechanism.[8] The electrons in the trap sites of Si_3N_4 are de-trapped through the hopping mechanism while the electron injection is suppressed by the high tunnel barrier at the FeO_x-GO/Si_3N_4 interface. As the applied bias voltage is further decreased, the current conduction is dominated by Schottky emission, which was confirmed by the linear relationships in the ln $|J|$-$|V|^{1/2}$ and the ln ($|J|/T^2$)-($1/kT$) plots[1], respectively (Fig. S5 b–c).

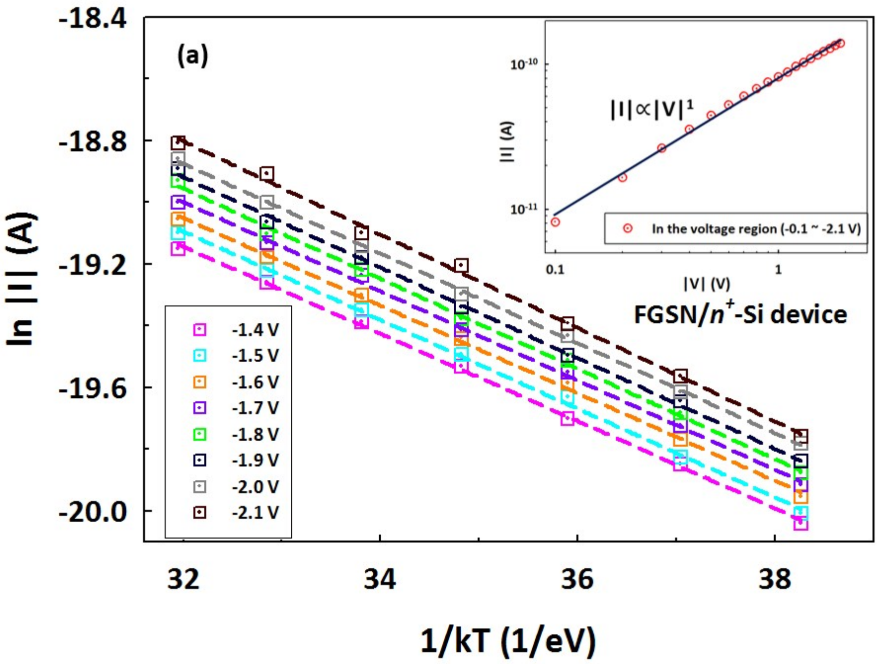

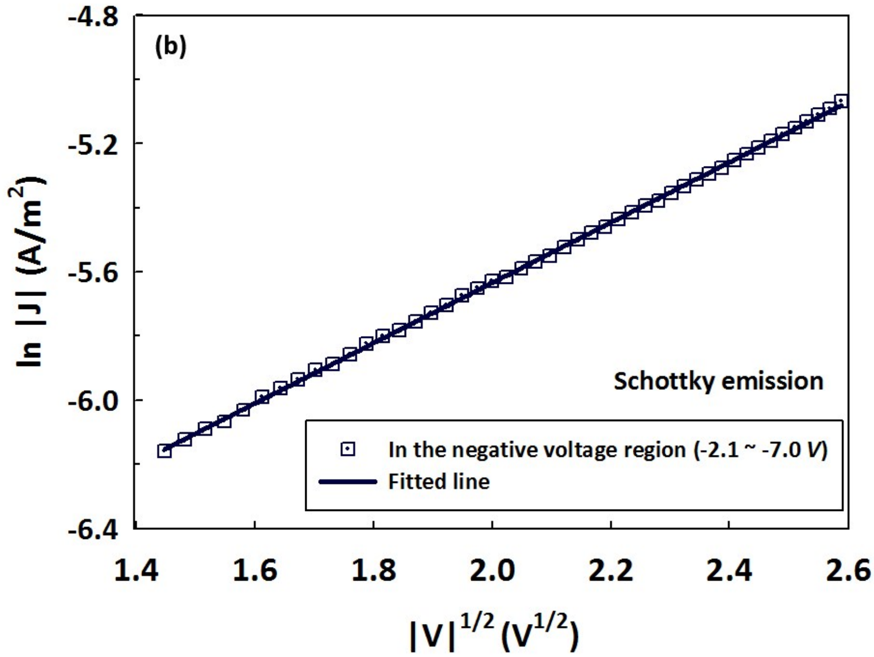

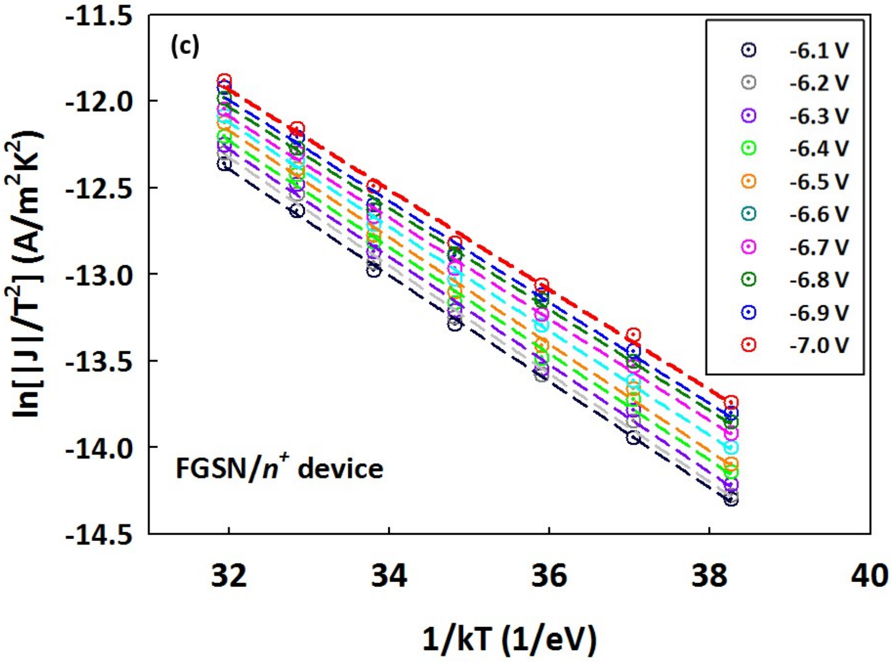

Fig. S5 a) Arrhenius plot (ln $|I|$-($1/kT$)) in the voltages ranging from −1.4 to −2.1 V. Inset figure is the log $|I|$-log $|V|$ plot in the voltages ranging from −0.1 to −2.1 V., b) The ln $|J|$-$|V|^{1/2}$ relation in the voltages ranging from −2.1 to −7.0 V, and c) The ln ($|J|/T^2$)-($1/kT$) characteristics in the voltages ranging from −6.1 to −7.0 V.

4. Electroforming process of FGSN/n^+ device

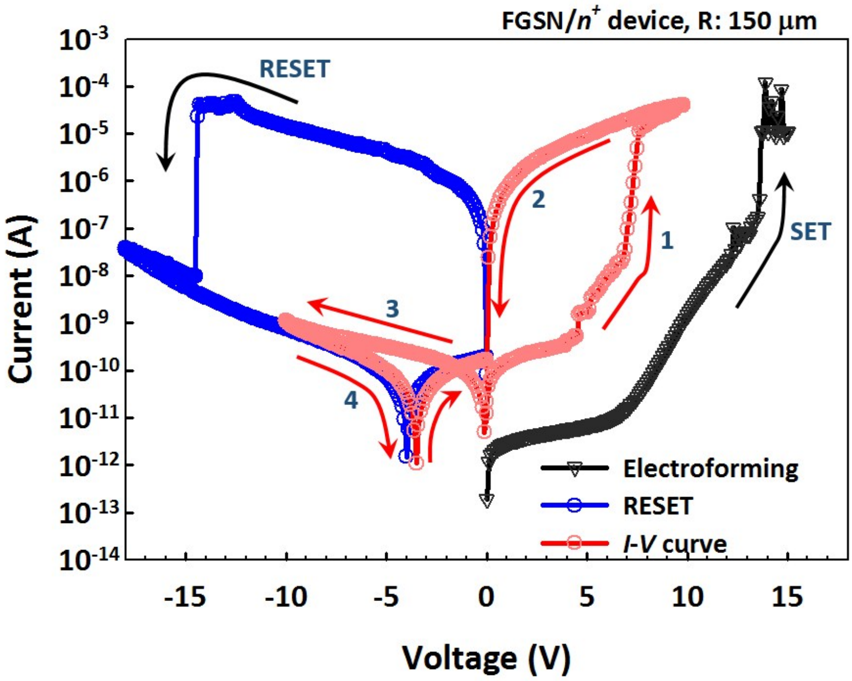

Fig. S6 Typical switching *I-V* characteristics of the FGSN/n^+ device together with the electroforming process and the following 1st RESET process.

5. RESET voltage of FGSN/n^+ device

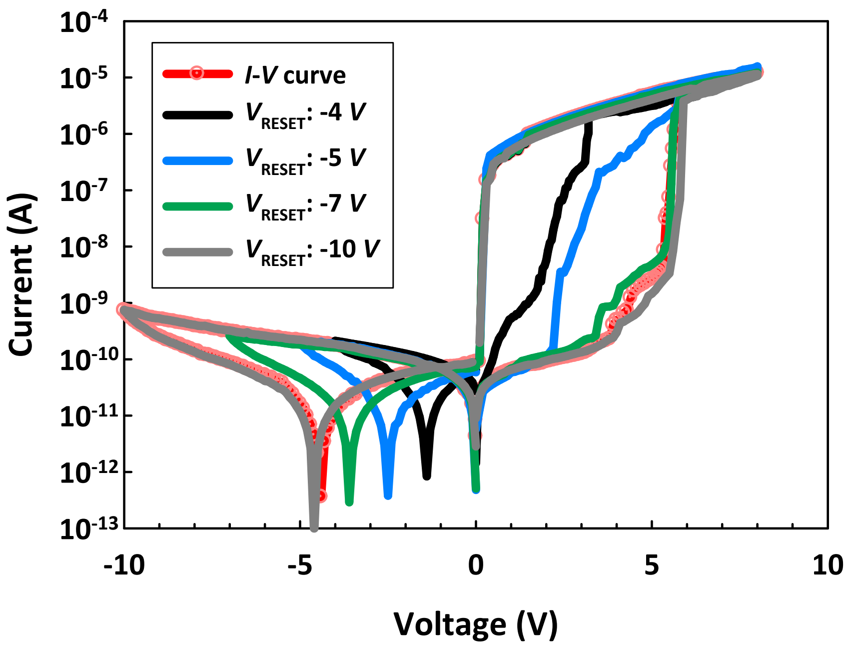

Fig. S7 The negative voltage amplitude-dependent *I-V* characteristics of the FGSN/n^+ device. The V_{RESET} of the device, which guarantees the reliable and repeatable full RESET operation, is −10 V.

6. Comparison of performance parameters of various self-rectifying RRAM devices

Table S2 The performance parameters of various vacuum-deposited and solution-processed RRAM devices exhibiting self-rectifying behaviors.

	Vacuum-deposited RRAM				**Solution-processed RRAM**			
Device Structure	Ag/a-Si/ p^+-Si	Ag/Na-ZnO/Si	$Pt/Ta_2O_5/HfO_2/TiN$	Pt/TaO_x/n-Si	$Pt/TiO_2/W$	Al/GO/Si	Al/ZnO/Al	FGSN/n^+
$\boldsymbol{I_{LRS}/I_{HRS}}$	10^6	10^3	10^3	10^4	400	110	10	1.6×10^4
$\boldsymbol{I_{LRS}/I_R}$	10^6	10^5	10^4	6.0×10^2	60	100	10	1.9×10^4
Retention (sec)	4.0×10^4	1.0×10^5	1.0×10^6	2.0×10^3	1.2×10^5	1.2×10^3	-	1.8×10^4
Endurance (cycles)	10^8	10^3	10^2	10^2	10^2	10^2	-	10^2
$\boldsymbol{\lvert V_{SET} \rvert}$ **(*V*)**	2.0	40.0	8.0	4.0	2.0	5.4	1.0	7.0
Reference	[9]	[10]	[11]	[12]	[13]	[14]	[15]	This work

7. Comparison of resistive switching characteristics of FGSN/n^+, GSN/n^+, FG/n^+, SN/n^+ devices

Table S3 The performance parameters and resistive switching characteristics of FGSN/n^+, GSN/n^+, FG/n^+, and SN/n^+ devices.

	FGSN/n^+	**GSN/n^+**	**FG/n^+**	**SN/n^+**
$\boldsymbol{V_{SET}}$ **(*V*)**	7.0	10.0	3.0	4.0
$\boldsymbol{I_{LRS}/I_{HRS}}$	1.6×10^4	5.5×10^2	4.0×10^4	2.0×10^5
Self-rectifying property	○	○	×	×

8. References

[1] A. Halilu, T. H. Ali, A. Y. Atta, P. Sudarsanam, S. K. Bhargava, and S. B. A. Hamid, *Energy Fuels*, 2016, **30**, 2216-2226.

[2] A. M. Jubb and H. C. Allen, *ACS Appl. Mater. Interfaces*, 2010, **2**, 2804-2812.

[3] O. Debieu, R. P. Nalini, J. Cardin, X. Portier, J. Perriere, and F. Gourbilleau, *Nanoscale Res. Lett.,* 2013, **8**, 31.

[4] Dielectric phenomena in solids, edited by K.-C. Kao, *Elsevier Academic*, San Diego, 2004.

[5] M. Molotskii, M. Naich, and G. Rosenman, *J. Appl. Phys.*, 2003, **94**, 4652-4658.

[6] H. Kato, H. Sato, Y. Ohki, K. S. Seol, and T. Noma, *J. Phys. Condens. Matter.*, 2003, **15**, 2197-2205.

[7] F. J.-Molinos, A. Palma, F. Gamiz, J. Banqueri, and J. A. L.-Villanueva, *J. App. Phys.,* 2001, **90**, 3396-3404.

[8] J. H. Yoon, S. J. Song, I.-H. Yoo, J. Y. Seok, K. J. Yoon, D. E. Kwon, T. H. Park, and C. S. Hwang, *Adv. Funct. Mater.,* 2014, **24**, 5086-5095.

[9] K.-H. Kim, S. H. Jo, S. Gaba, and W. Lu, *Appl. Phys. Lett.*, 2010, **96**, 053106.

[10] J. Qi, J. Huang, D. Paul, J. Ren, S. Chu, and J. Liu, *Nanoscale*, 2013, **5**, 2651-2654.

[11] J. H. Yoon, S. J. Song, I.-H. Yoo, J. Y. Seok, K. J. Yoon, D. E. Kwon, T. H. Park, and C. S. Hwang, *Adv. Funct. Mater.,* 2014, **24**, 5086-5095.

[12] S. Gao, F. Zeng, F. Li, M. Wang, H. Mao, G. Wang, C. Song, and F. Pan, *Nanoscale*, 2015, **7**, 6031-6038.

[13] K. P. Biju, X. Liu, J. Shin, I. Kim, S. Jung, M. Siddik, J. Lee, A. Ignatiev, and H. Hwang, *Curr. Appl. Phys.*, 2011, **11**, S102-S106.

[14] S. M. Jilani, T. D. Gamot, P. Banergi, and S. Chakraborty, *Carbon*, 2013, **64**, 187-196.

[15] A. Kathalingam, H.-S. Kim, S.-D. Kim, H.-M. Park, and H.-C. Park, *Mater. Lett.*, 2015, **142**, 238-241.